Jurnal Teknologi Perikanan dan Kelautan Vol. 16 No. 2 May 2025: 160-172 *ISSN 2087-4871*
DOI: https://doi.org/10.24319/jtpk.16.160-172 *EISSN 2549-3841*

EVALUATION OF NUSANTARA 3 REMOTELY OPERATED VEHICLE (N3-ROV) SPECIAL REPORT OF PERFORMANCE AND STABILITY IN VARIOUS WATER CONDITIONS

EVALUASI KINERJA DAN STABILITAS NAVIGASI NUSANTARA 3 *REMOTELY OPERATED VEHICLE* (N3-ROV) DALAM LINGKUNGAN PERAIRAN BERBEDA

Xavercius Cezar Pratama*, Indra Jaya, Muhammad Iqbal
Study Program of Marine Science and Technfology, Faculty of Fisheries and Marine Sciences, IPB University,
Jl. Agatis, IPB Dramaga Campus, Bogor 16680, Indonesia
*Corresponding author: xaverciusc@gmail.com

(Received June 1, 2024; Revised November 22, 2024; Accepted April 5, 2025)

ABSTRACT

Vast marine resources require underwater observation and exploration, but conventional diving methods have many risks. Therefore, developing underwater technology such as Remotely Operated Underwater Vehicles (ROV) is essential to reduce the risk. However, the unpredictable underwater environment requires ROV performance testing before optimal use. Therefore, this study was conducted to test the performance of the N3-ROV, determine its specific specifications, and design a control system and video acquisition so that it can be an alternative for underwater observation and exploration. The N3-ROV has dimensions of 61x65x34 cm, a total weight of 13 kg, with a buoyancy of 128.4 kg.m/s^2, with surface control using a gamepad connected to a laptop. Performance tests were carried out in two different environments, a pool environment and a field environment. The N3-ROV has a straight movement in the pool environment with an error of 0° and in the field environment of 1.7° with speeds of 76.6 cm/s and 77.2 cm/s, respectively. The descent motion in both environments is different, where in the pool environment, the descent motion has a delay and error of 9.7 seconds and 94.1°, respectively, compared to the field environment of 3.9 seconds and 48.8°. The delay and error in the turning motion in the pool environment are higher than in the sea environment. The gliding motion in the pool environment has a slower surfacing speed compared to the field environment.

Keywords: evaluation, N3-ROV, performance, underwater technology

ABSTRAK

Sumber daya laut yang luas memerlukan observasi dan eksplorasi bawah air, tetapi metode konvensional penyelaman memiliki banyak risiko. Oleh karena itu, pengembangan teknologi bawah air seperti *Remotely Operated Underwater Vehicle* (ROV) sangat penting untuk mengurangi risiko. Namun, lingkungan bawah air yang tidak terduga memerlukan pengujian kinerja ROV sebelum digunakan secara optimal. Oleh karena itu, dilakukan penelitian ini untuk menguji kinerja N3-ROV, mengetahui spesifikasi khususnya, serta merancang sistem kendali dan akuisisi video agar dapat menjadi alternatif untuk observasi dan eksplorasi bawah air. N3-ROV memiliki dimensi 61x65x34 cm, berat total 13 kg dengan daya apung sebesar 128,4 kg.m/s^2 dengan kendali di permukaan menggunakan *gamepad* yang terhubung ke laptop. Uji kinerja dilakukan pada dua lingkungan yang berbeda, lingkungan kolam dan lingkungan lapang. N3-ROV memiliki pergerakan lurus pada lingkungan kolam dengan *error* sebesar 0° dan pada lingkungan lapang sebesar 1,7° dengan kecepatan berturut-turut 76,6 cm/s dan 77,2 cm/s. Gerak turun pada kedua lingkungan berbeda dimana pada lingkungan kolam gerak turun memiliki *delay* dan *error* berturut-turut sebesar 9,7 detik dan 94,1° dibandingkan dengan lingkungan lapang 3,9 detik dan 48,8°. *Delay* dan *error* pada gerak berbelok di lingkungan kolam lebih tinggi dibandingkan lingkungan laut. Gerak gliding pada lingkungan kolam memiliki kecepatan surfacing yang lebih lambat dibandingkan dengan lingkungan lapang.

Kata kunci: kinerja, N3-ROV, spesifikasi, teknologi bawah air

INTRODUCTION

The ocean, as a vast natural resource, plays a crucial role in human life, yet optimizing its potential remains complex. Diving for ocean exploration, although used for centuries, faces challenges such as deep-sea pressure and navigation hazards (Xia *et al.* 2022). As a solution to these risks, Unmanned Underwater Vehicles (UUVs), particularly Autonomous Underwater Vehicles (AUVs) and Remotely Operated Underwater Vehicles (ROVs), have been developed. ROVs, which are manually operated and tethered by cables, have proven to be valuable in various applications, including underwater inspections (Manullang *et al.* 2020). Previous studies have applied ROVs for monitoring aquatic environments, coral reefs, industrial activities, and fish farming (Adhipramana *et al.* 2020; Payung and Zain 2021; Septian *et al.* 2019; Betancourt *et al.* 2020). However, the complexity of the marine environment presents significant challenges. For instance, movement disturbances caused by ocean currents can create thrust or drag forces that directly interact with the vehicle, potentially disrupting its movement (Fariqi *et al.* 2021).

The development of the N3-ROV was initiated as a solution to this issue by adopting a microcomputer as the main control center and reconfiguring the number and position of motors. One of the advantages of the N3-ROV compared to previous ROVs is the use of the Raspberry Pi 3 microcomputer as the main control system, along with a more flexible motor configuration tailored to operational needs. Therefore, this study aims to evaluate the performance of the N3-ROV, determine its specific features, and design a control and video acquisition system so that it can serve as an alternative for underwater observation and exploration. The research consists of three stages: mechanical analysis, control, video acquisition system design, and analysis of ROV behavior in two environments.

METHODS

The research was conducted from February to July 2023. The design and development of the vehicle's working system were carried out at the Marine Instrumentation and Robotics Workshop, Department of Marine Science and Technology, Faculty of Fisheries and Marine Sciences, IPB University. The vehicle trials were conducted at the IPB Aquatic Center. Field testing was carried out at the IPB Sea Farming Center in the area around the floating net cages (KJA), in Semak Daun Island, Thousand Islands, Jakarta. The hardware and software used in the research are shown in Table 1.

The details of the vehicle used in this research are presented in Table 2, and its physical form can be seen in Figure 1. Performance data of the vehicle in two different environments will later be used for evaluation.

Figure 2 illustrates the research flow, which consists of three stages: mechanical analysis, control system design, and ROV behavior analysis. The mechanical analysis produces two outputs: the specific specifications of the vehicle and the number of Degrees of Freedom (DoF) it can achieve. The second stage involves designing the video acquisition and control system programs based on the identified DoF. The third stage is the analysis of ROV behavior, starting with testing the control system and resulting in performance data of the vehicle in two different environments, which will later be used for evaluation.

Mechanical analysis

The mechanical analysis is divided into two outputs: the specific specifications of the vehicle and the number of Degrees of Freedom (DoF). The specific specifications include calculations of buoyant force, determination of the center of buoyancy and center of gravity, and estimation of the vehicle's operating duration.

Buoyancy

$$Fa = \rho . g . V_b$$

Description:
Fa = Buoyancy ($kg.m/s^2$)
ρ = Fluid density (kg/m^3)
g = Gravitational force (m/s^2)
V_b = Object volume (m)

This formula states that the buoyant force experienced by an object in a fluid is directly proportional to the volume of fluid displaced by the object, allowing us to measure the water displacement generated by the vehicle to determine its buoyant force (Kumar *et al.* 2023) using the following equation:

$$V_b = \Delta V = v_1 - v_0$$

Description:
V_b = Object volume (cm^2)
v_0 = Initial volume of water in the container (cm^2)
v_1 = Volume of water in the container with the submerged vehicle (cm^2)

The condition of the vehicle can be determined using a comparison formula between the object's weight (W) and the buoyant force (Fa). The ratio between W and Fa represents the net force acting on the object. The formula for the net force on the object can be seen in the following equation:

$$W = Fa$$

Description:
Fa = Buoyancy ($kg.m/s^2$)
W = Weight force of the object ($kg.m/s^2$)
If the net force acting on the object is positive (W<Fa), the vehicle will float; if it is negative (W>Fa), it will sink; and if it is neutral or zero (W=Fa), the vehicle will hover in the water (Hidayat *et al.* 2020).

Center of buoyancy (*CB*) *and center of gravity* (*CG*)

The center of buoyancy (CB) is the point at which the buoyant force acts on a submerged object. This buoyant force (F) is the upward force caused by the fluid displaced by the object. In addition, there is a gravitational force (CG) that acts downward through the object's center of mass (W) (Bajo *et al.* 2020).

Operational or runtime duration of the vehicle

The operational duration can be calculated by determining the total battery capacity and the electrical consumption of all components used. The calculation can be performed using the following equation (Prabowo *et al.* 2022):

$$Operational\ duration = \frac{Battery\ capacity}{Total\ current\ of\ electronic\ components}$$

ROV behavior analysis

Forward movement analysis

The forward movement test is conducted to evaluate the vehicle's ability to move in a straight line. The vehicle moves forward in 8 seconds, repeated four times using different PWM (Pulse Width Modulation) values on the motors to determine the setting that achieves the smallest movement error. Error (e) is defined as the difference between the ROV direction in the position it should be in (d_0) and the ROV direction in the actual position after 8 seconds (d_1), calculated using the following equation:

$$e = d_1 - d_0$$

Description:
e = Error (°)
d_0 = ROV direction on the position it should be in (°)
d_1 = ROV direction on actual position (°)

Tabel 1. Hardware and software used in the research.

Hardware/Software	Type	Number	Information
Laptop	Asus TUF Gaming F15	1	Control center and data processing
Vehicle	N3-ROV	1	Tested vehicle
Router	TP-LINK EN020-F5	1	Creating a connecting network route
Gamepad	MT-830S	1	Vehicle controller
Programming language	Python 3.9.6	1	Basic control logic and video acquisition of the vehicle
	HTML	1	Control website structure
	CSS	1	User interface
	Java Script	1	Website functionality
Software	VNC Viewer 6.22.826	1	Raspberry pi visual access
	Visual Studio Code 1.83.0	1	Code editor

Table 2. Specifications of weight, dimensions, and camera of the N3-ROV vehicle.

Type	Information
Weight	13 kg
Dimensions	61x65x34 cm
Camera	Webcam Logitech B525

Figure 1. The physical form of the N3-ROV vehicle.

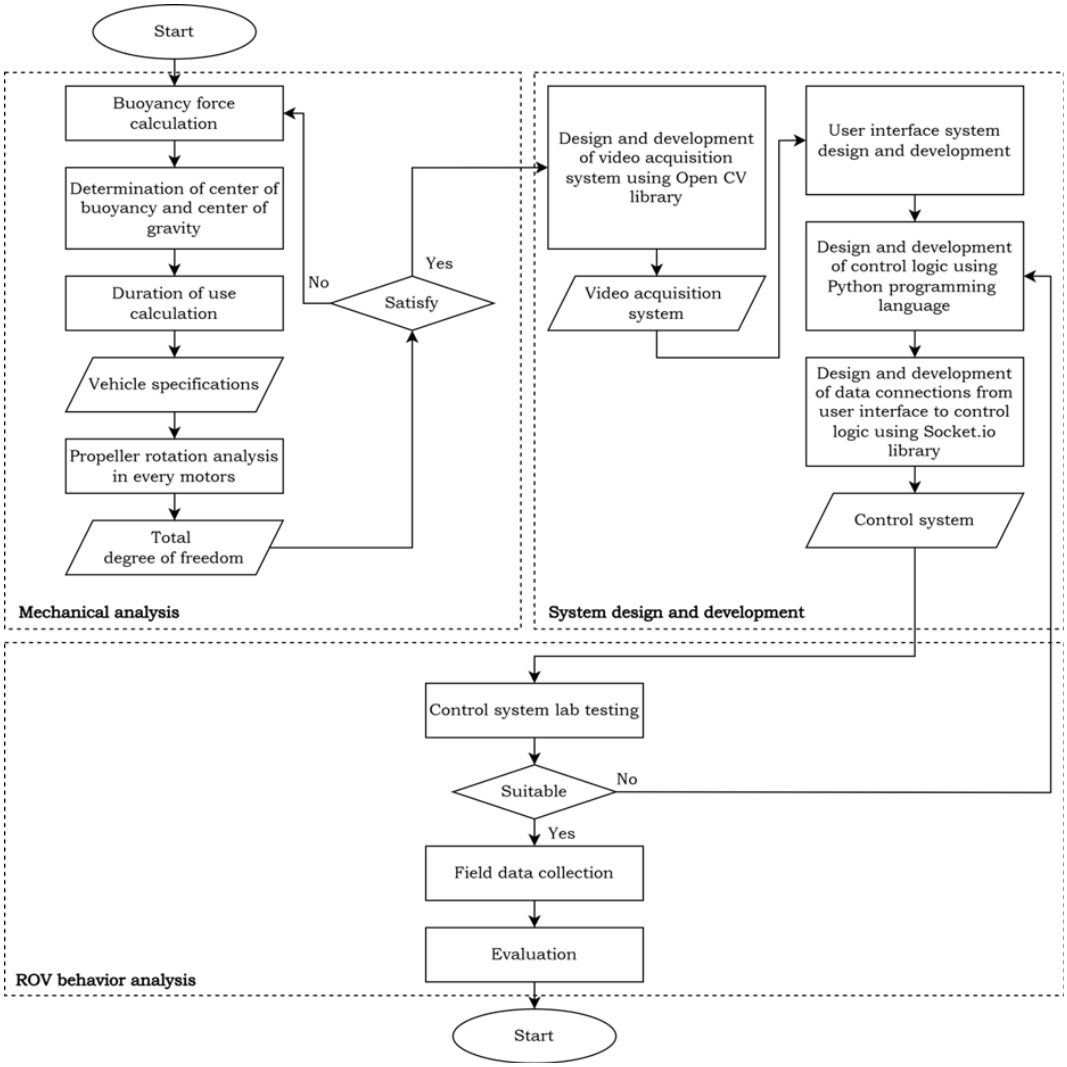

Figure 2. The procedural flow diagram of the research begins with mechanical analysis, system design and development, ROV behavior analysis, and ends with evaluation.

Turning movement analysis

The turning movement test begins by commanding the vehicle to turn right until it reaches a 90° position. In practice, there is a delay (D) and an error (e) before reaching the actual position. Delay (D) is the time difference between the expected position (t_0) and the actual position (t_1). Error is the difference between the direction at the expected position (d_0) and the actual position (d_1). The delay and error can be formulated using the following equation:

$$e = d_1 - d_0$$

$$D = t_1 - t_0$$

Description:
e = Error (°)
d_0 = ROV direction on expected position (°)
d_1 = ROV direction on actual position (°)
D = Delay (s)
t_0 = ROV time in expected position (s)
t_1 = ROV time in actual position (s)

Descent movement analysis

The descent movement analysis examines the delay and error when the vehicle moves downward. The vehicle is commanded to descend to a specific depth under two different conditions: 8 seconds in the laboratory environment and 10 seconds in the field environment, due to the depth limitations in the lab. Delay (D) is the time difference between the expected depth (p_0) and the actual depth (p_1). Error (E) is the difference between the expected and actual depth. These delay and error values can be formulated using the following equation:

$$E = p_1 - p_0$$

$$D = t_1 - t_0$$

Description:
E = Error (cm)
p_0 = ROV depth at 8 or 10 seconds (cm)
p_1 = ROV deepest depth (cm)
D = Delay (s)
t_0 = ROV time at depth at 8 or 10 seconds (s)
t_1 = ROV time at deepest depth (s)

Gliding movement analysis

The gliding movement test analyzes the vehicle's surfacing speed (Q) from a certain depth. First, the vehicle performs a descent motion to a depth (P). The maximum depth during the descent is tested in three trials with different depths: in the lab environment, the depth is 80 cm, 120 cm, and 170 cm, and in the field environment the depth is 100 cm, 200 cm, and 300 cm. In the second movement, the vehicle moves forward until it reaches the surface (T). To determine the surface speed, the following equation is formulated:

$$Q = \frac{P}{T}$$

Description:
T = Time needed by the ROV to reach the surface from the deepest depth (s)
P = ROV deepest depth (cm)
Q = Surfacing speed (cm/s)

RESULTS AND DISCUSSION

Mechanical analysis

The mechanical analysis produces two outputs, namely, the specific specifications of the vehicle and the number of Degrees of Freedom (DoF) the vehicle can perform. The specific specifications include detailed dimensions, determination of the center of buoyancy and center of gravity, and calculation of the vehicle's runtime. The number of DoF is determined based on the motor positions and the direction of the propeller rotation.

Specific specifications of the vehicle

A detailed overview of the N3-ROV's dimensions can be seen in Figure 3, including its length, width, total height, the distance between each motor, as well as the center points of buoyant force and gravitational force. The overall dimensions of the vehicle are 61 cm in length, 65 cm in width, and 34 cm in height, with the center of buoyant force and gravitational force located 30 cm from the rear of the vehicle. These center points can be determined by referring to the stability of submerged objects as described by Bajo *et al.* (2020) and Rivalji (2013).

Based on the concept of submerged object stability, if a designated point causes the object to remain balanced, that point is identified as the CG (Center of Gravity) or CB (Center of Buoyancy). CG and CB must have a specific relationship. If the CG is located directly below the CB, the object will tend to remain upright and stable. However,

if the CG is higher than the CB, the object will tend to tip over or become unstable. Conversely, if the CG is too far below the CB, the object can become overly stable and difficult to maneuver. Therefore, maintaining a balanced position between the CG and CB is crucial for ensuring the stability of an object submerged in a fluid.

The buoyancy calculation of the vehicle can be performed using Archimedes' Principle and the concept of water displacement to determine the total volume of the vehicle, as follows:

$$V_b = v_1 - v_0$$

$$V_b = (38\ cm \times 78\ cm \times 40.2\ cm) - (38\ cm \times 78\ cm \times 35.5\ cm)$$

$$V_b = 119.2\ cm^3 - 106.1\ cm^3 = 13.1\ cm^3$$

The obtained volume can be used in the following Archimedes' Law equation:

$$Fa = \rho . g . Vb$$

$$Fa = 1000\ kg/m^3 \times 9.8\ m/s^2 \times 0.0131\ m^3$$

$$Fa = 128.4\ kg.m/s^2$$

The buoyancy of the vehicle is determined to be 128.4 kg.m/s^2.

The condition of the vehicle can be determined using the following equation:

$$W = Fa$$

$$13\ kg.9.8\ m/s^2 = 128.4\ kg.m/s^2$$

$$127.4\ kg.m/s^2 < 128.4\ kg.m/s^2$$

Since the value of W is smaller than Fa, the vehicle is in a floating condition and will rise to the surface on its own if submerged at a certain depth.

The operational or runtime duration of the vehicle can be estimated based on the calculation of the electronic components installed on the vehicle. The total current produced by the electronic components is 1,120 mA, with a total power of 4.4 W. Detailed electrical specifications of the components can be seen in Table 3.

The total current used by the vehicle is known, and the power load supplied by the battery can be calculated, allowing the runtime duration of the vehicle to be determined as follows:

Runtime = Battery Capacity / Total Current = 3,300 mAh / 1,139.25 mA = 2.89 h or 2 hours 53 minutes and 4 seconds.

Motor position

The position of the motor (M) on the vehicle significantly affects its movement capabilities and the number of Degrees of Freedom (DoF) it can perform. The N3-ROV has 8 motors, divided into two groups, vertical and horizontal. The vertical position consists of 4 motors (numbers 1-4) with the inlets facing upward when the propellers rotate clockwise, while the horizontal position consists of 4 motors (numbers 5-8) with inlets aligned in the direction of the arrows shown in Figure 4.

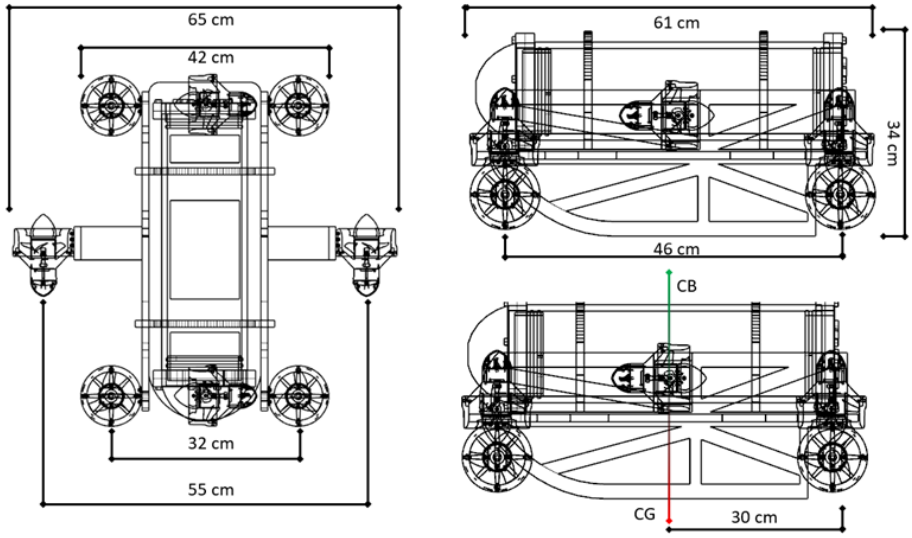

Figure 3. Overall dimensions and details of the distance between the motors of the N3-ROV vehicle.

Table 3. Electrical specifications of the main components of the N3-ROV vehicle.

Module	Amount	Voltage (V)	Current (mA)	Power (W)
Arduino Mega 2560	1	5	200	1
LCD 16x2	1	5	120	0.6
Blue Robotic ESC*	8	10	400	0.5
Compass CMPS 12	1	3.3	18	0.0594
Blue Robotic Bar30 Depth Sensor	1	5	1.25	0.0625
Total		**1139.25**		**4.5219**

*Assuming all eight ESCs are used simultaneously and continuously with PWM 1550

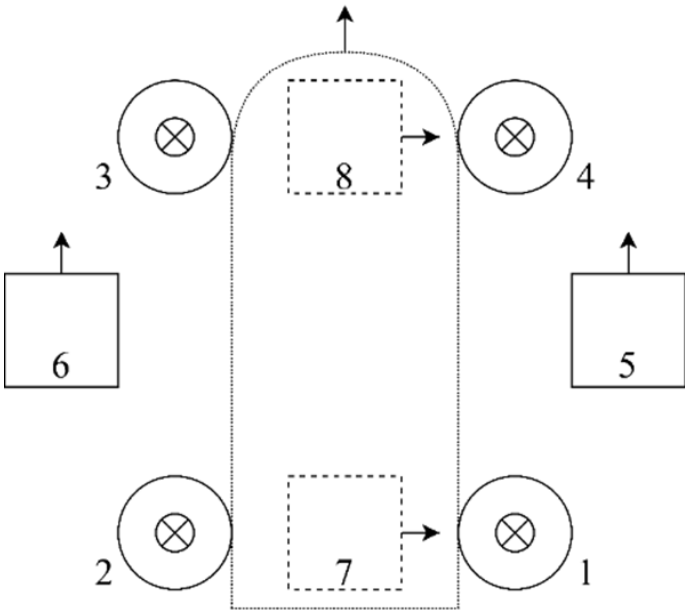

Figure 4. Motor position and motor inlet direction on the N3-ROV vehicle.

Propeller rotation

The rotation of the propellers is divided into two types, clockwise (CW) and counterclockwise (CCW). This difference in rotation affects the direction of thrust generated by the motors on the ROV. CW rotation directs the motor's thrust from the inlet to the outlet as shown in Figure 4, while CCW rotation does the opposite. Therefore, the propeller's rotation direction influences the ROV's movement (Atali 2022), and based on this, a maneuverability table can be generated, as shown in Table 4.

Table 4 shows that the N3-ROV is capable of performing 6 Degrees of Freedom (DoF) by utilizing each motor and the varying directions of propeller rotation. This is also in line with the findings of Kabanov *et al.* (2021), which state that by knowing the number of motors and the thrust generated by each propeller, the number of DoF of the vehicle can be determined.

System design and development

The design and development of the vehicle system are divided into two parts: the design and development of the user interface (UI) and the control logic. The UI design and development cover the video acquisition system as well as supporting control parameters such as depth, direction, and pitch and roll. Meanwhile, the control logic design focuses on the functionality of the connection between the control device and the vehicle.

User interface (UI)

The UI design consists of three components, where HTML (Hypertext Markup Language) serves as the backbone and structure for designing the web page, CSS (Cascading Style Sheets) is used to design the layout and appearance of the HTML elements, and JS (JavaScript) makes

the web page more interactive and dynamic. The design scheme of the HTML elements for the UI layout can be seen in Figure 5.

The N3-ROV control UI includes several control parameters, such as depth and direction, as well as pitch and roll. The control UI for underwater vehicles is a key element in operations (Ray *et al.* 2020), where the vehicle is used for various tasks such as seafloor exploration, underwater environmental monitoring, and underwater structure maintenance. Depth data helps determine the vehicle's position relative to the water surface, while directional information assists in navigation. Additionally, pitch and roll are important parameters that provide insight into the vehicle's orientation and help maintain its balance.

Control logic

The control logic design uses the Python programming language with several libraries. Key libraries include Flask, a web framework for building web applications with Python; Flask-Serial, which simplifies serial communication; Flask-SocketIO for real-time, two-way communication; and cv2 as a computer vision library. The next step, after successful data transmission using Flask-SocketIO, is to design the main control system by mapping the button layout on the gamepad. This layout is crucial to ensure efficient and safe operation of the vehicle. ROV gamepads are typically equipped with buttons that have specific functions, such as controlling movement, depth, speed, and camera. The detailed layout of the control buttons can be seen in Figure 6.

Table 4. N3-ROV maneuvers based on motor position and propeller rotation direction.

M1	M2	M3	M4	M5	M6	M7	M8	Condition	Description
CW	CW	CW	CW	-	-	-	-	Ascending	Heaving
CCW	CCW	CCW	CCW	-	-	-	-	Descending	Heaving
-	-	-	-	CW	CW	-	-	Forward	Surging
-	-	-	-	CCW	CCW	-	-	Backward	Surging
-	-	-	-	-	-	CCW	CCW	Strafe left	Swaying
-	-	-	-	-	-	CW	CW	Strafe right	Swaying
-	-	-	-	-	-	CCW	CW	Turn right	Yaw
-	-	-	-	-	-	CW	CCW	Turn left	Yaw
CCW	CCW	CW	CW	-	-	-	-	Pitch up	Pitch
CW	CW	CCW	CCW	-	-	-	-	Pitch down	Pitch
CW	CCW	CCW	CW	-	-	-	-	Roll right	Roll
CCW	CW	CW	CCW	-	-	-	-	Roll left	Roll

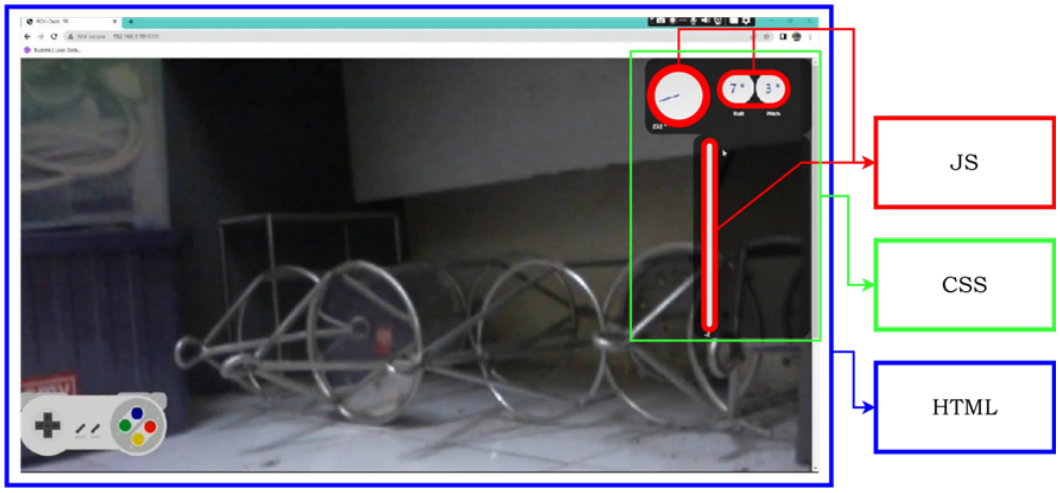

Figure 5. CSS, JS, and HTML schemes in UI design.

Figure 6. Layout of control buttons on the gamepad.

ROV behavior analysis

Forward movement analysis

Forward movement analysis in the pool showed the lowest error in the fourth trial (U4) and the highest in the third (U3) (Table 5). The movement pattern of the vehicle (Figure 7a) indicates that this was caused by using different coefficients on the right and left motors in each trial. Various coefficients were applied to achieve the lowest error (Table 6). In the field (Figure 7b), straight-line movement showed greater error, again with U4 being the most accurate and U3 the least (Table 5). The increased error is likely caused by external factors such as tidal currents, which generate thrust or resistance forces affecting the vehicle's motion (Fariqi *et al.* 2021). The vehicle also moved faster in the field, influenced by environmental conditions, including currents (Konoplin *et al.* 2022). In this location, tidal currents have been recorded at approximately 0.09 cm/s, contributing to the observed variations (Bramana *et al.* 2014).

Descent movement analysis

The descent movement analysis in the pool (Figure 8) showed an average delay of 9.7 seconds with a depth error of 94.1 cm (Table 7). This indicates that the vehicle continued descending during the delay period. The cause was the nearly equal buoyant force and gravitational force acting on the vehicle. The field test (Figure 9) showed an average delay of 3.9 seconds and an error of 48.8 cm (Table 7). This was due to the difference in water density, which resulted in a greater buoyant force on the vehicle compared to the pool (Edison 2021). A higher water density means a stronger upward force acting on the vehicle, which in turn affects the vehicle's descent movement.

Table 5. Results of forward movement error analysis in the pool and in the field.

Heading (°)	Test							
	1		2		3		4	
	Pool	Field	Pool	Field	Pool	Field	Pool	Field
Start	213.8	213.2	213.8	213.4	213.8	213.8	213.8	213.4
Stop	215.4	206.4	213.9	210.8	204.1	199.7	213.8	211.7
Error	1.6	6.8	0.11	2.6	9.7	14.1	0	1.7

Table 6. Difference in speed coefficient of right and left motor for forward movement in each test.

Test	PWM			Speed (cm/s)	
	Base	Right	Left	Pool	Field
1	1550	1560	1555	76.6	77.2
2	1550	1560	1554		
3	1550	1559	1555		
4	1550	1561	1554		

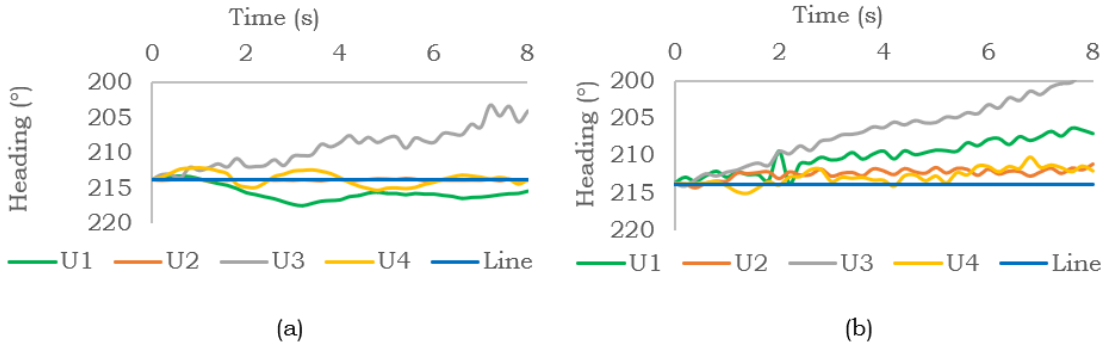

Figure 7. The pattern of forward movement direction values in the pool (a) and in the field (b); Line (Initial direction), U (Test-th).

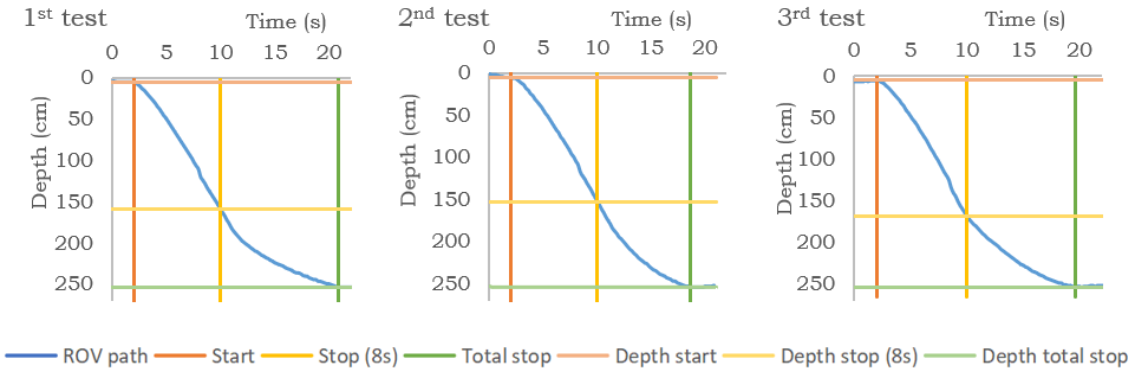

Figure 8. Graph of the depth value of downward movement in the pool.

Table 7. Results of analysis of delay and error of descending motion in the pool and in the field.

	Time (s)						Depth (cm)					
	Pool			Field			Pool			Field		
	U1	U2	U3	U1	U2	U3	U1	U2	U3	U1	U2	U3
Start	2	2.2	2	1.2	1.8	2.8	4.1	5.1	4.1	10.2	7.2	11.3
Stop	10	10.2	10	11.2	11.8	12.8	158.5	152.4	167.7	128.9	126.8	127.9
Total stop	20.8	18.8	19.6	15.6	15.8	16.2	253.6	253.6	253.6	181.0	182.1	166.7
Delay /error	10.8	8.6	9.6	4.4	4	3.4	95.1	101.2	85.9	52.2	55.2	38.9
Average		**9.7**			**3.9**			**94.1**			**48.8**	

Information: U1 (1st test), U2 (2nd test), and U3 (3rd test)

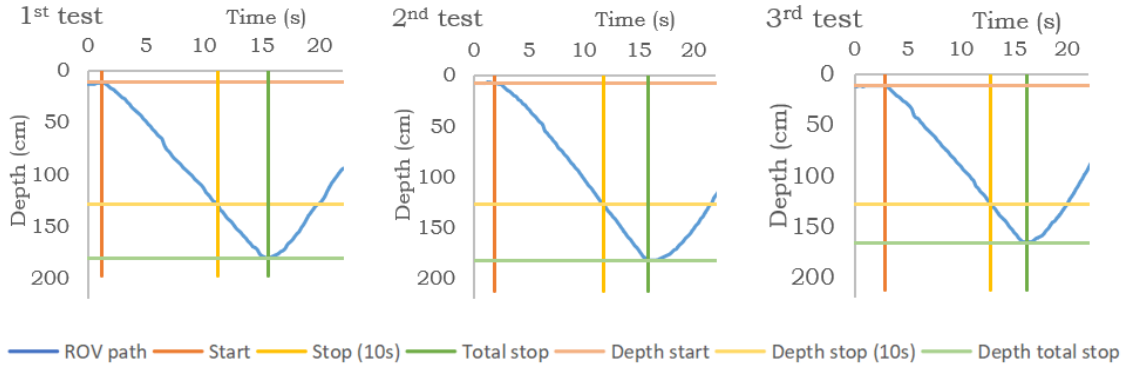

Figure 9. Graph of the depth value of downward movement in the field.

Turning movement analysis

Turning movement analysis in the pool (Figure 10) showed an 11.3 seconds delay and a 71° error (Table 8). The delay was the time between the stop command and actual stopping, while the error was the directional difference from the command to the final position. In the field test (Figure 11), the delay and error were smaller, 4.1 seconds and 14° (Table 8). This difference was due to external factors in open water, such as currents, water density, and tides, which create thrust or drag forces that can disrupt movement. In the pool, without such factors, the vehicle moved longer along the same path, causing larger errors.

Gliding movement analysis

Gliding motion analysis from three trials (U1, U2, U3) showed depth differences due to the pool's limited depth. The pool test (Figure 12a) recorded a lower average surfacing speed than the field test (Figure 12b). Average surfacing speed (Q) was calculated by dividing descent depth (P) by ascent time (T). In the pool, the average speed was 10.2 cm/s, while in the field it was 11.7 cm/s (Table 9), due to higher water density in the field, which increased the buoyant force and thus the surfacing speed.

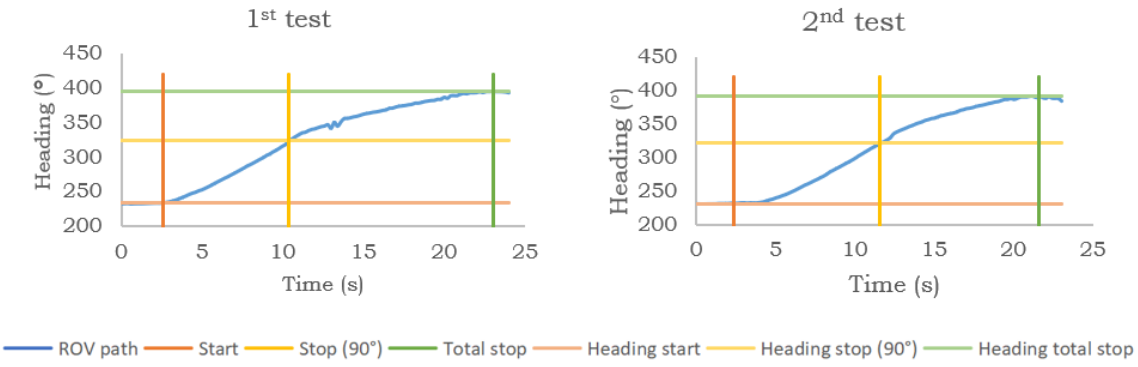

Figure 10. Graph of heading direction values in the pool.

Table 8. Results of analysis of delay and turning error in the pool and in the field.

	Time (s)				**Heading (°)**			
	Pool		**Field**		**Pool**		**Field**	
	U1	**U2**	**U1**	**U2**	**U1**	**U2**	**U1**	**U2**
Start	2.6	3.8	2.8	2.8	223.4	231	219.5	223.4
Stop (90°)	10.4	11.6	12.4	12.4	313.4	321	309.5	313.4
Total stop	23	21.6	16.6	16.6	395	391.7	324.7	326.3
Delay/error	12.6	10	4.2	4.2	71.3	70	15.2	12.9
Average delay/error	**11.3**		**4.2**		**71**		**14.1**	

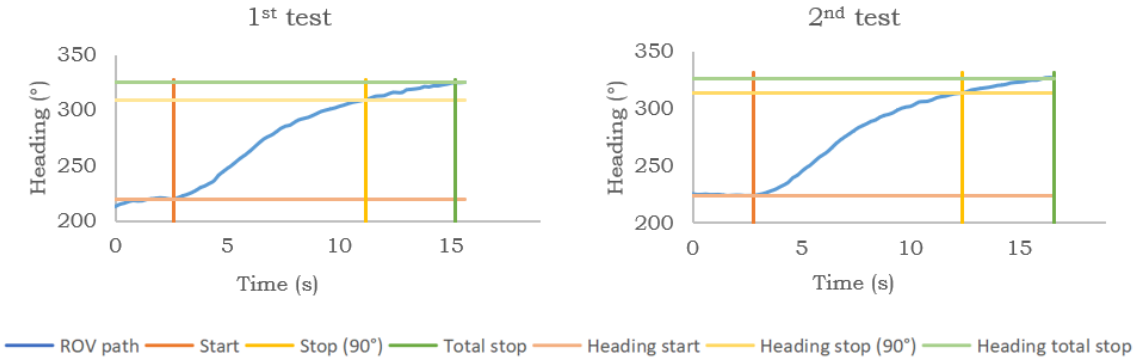

Figure 11. Graph of heading direction values in the field.

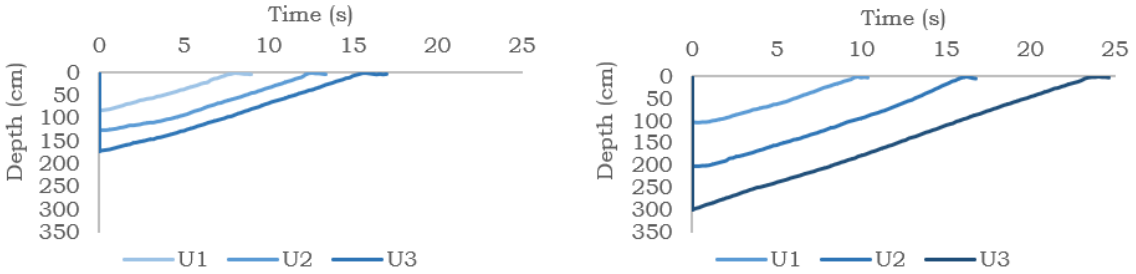

Figure 12. Glide movement patterns in the pool (a) and in the field (b).

Table 9. Results of the analysis of delay and error in gliding movement in the pool and field.

Test	Pool			Field		
	P (cm)	T (s)	Q (cm/s)	P (cm)	T (s)	Q (cm/s)
1	80	8	10.2	100	9.8	10.2
2	124	12.6	9.8	200	16.2	12.3
3	170	15.6	10.9	300	24	12.5
Average Q			**10.2**			**11.7**

CONCLUSION

The N3-ROV, with a buoyant force of 128.4 kg.m/s² and gamepad control via a laptop, was evaluated for underwater exploration, observation, and marine research support. Structurally, it operates with four active degrees of freedom, as the CG and CB positioning limit certain maneuvers. Tests in the pool and open water showed environment-dependent variations: in the pool, the ROV had greater angular error, response delays during descent and turns, and reduced surfacing speed, suggesting constraints in confined or resistive fluids. However, it maintained high directional accuracy, achieving 0° angular error at 76.6 cm/s in the pool and 1.7° at 77.2 cm/s in open water. Despite maneuverability limits from its configuration, the N3-ROV shows strong potential for precise, stable linear movement. These findings validate its foundational capability for underwater observation, with further improvements in attitude control and degrees of freedom expected to enhance performance in complex marine environments.

REFERENCES

Adhipramana M, Mardiati R, Mulyana E. 2020. Remotely Operated Vehicle (ROV) Robot for Monitoring Quality of Water Based on IoT. *2020 6th International Conference on Wireless and Telematics (ICWT), 03-04 September 2020, Yogyakarta, Indonesia*. IEEE.

Atali G. 2022. Prototyping of a Novel Thruster for Underwater ROVs. *International Journal of Applied Mathematics, Electronics and Computers*. 10(1): 11-14. DOI: https://doi.org/10.18100/ijamec.1045491.

Bajo JM, Patow G, Delrieux CA. 2020. Realistic Buoyancy Model for Real-Time Applications. *Computer Graphics Forum*. 39(6): 217-231. DOI: https://doi.org/10.1111/cgf.14013.

Betancourt J, Coral W, Colorado J. 2020. An Integrated ROV Solution for Underwater Net Cage Inspection in Fish Farms Using Computer Vision. *SN Applied Sciences*. 2(1946): 1-15. DOI: https://doi.org/10.1007/s42452-020-03623-z.

Bramana A, Damar A, Kurnia R. 2014. Estimasi Daya Dukung Lingkungan Keramba Jaring Apung di Perairan Pulau Semak Daun Kepulauan Seribu, DKI Jakarta. *Jurnal Teknologi Perikanan dan Kelautan*. 5(2): 163-172. DOI: https://doi.org/10.24319/jtpk.5.161-170.

Edison E. 2021. Perancangan Sepeda Air untuk Kendaraan Wisata Alam Lembah Harau. *Rang Teknik Journal*. 4(2): 339-347. DOI: https://doi.org/10.31869/rtj.v4i2.2635.

Fariqi M, Rahmat MB, Ahmad ZM. 2021. Implementasi *Heading*

Hold dan *Invers Kinematics* pada ROV Menggunakan Metode PID. *Journal Conference on Automation Engineering and Its Application*. 1: 66-69.

Hidayat DS, Rakhmat C, Fattah N, Rochyadi E, Nandiyanto ABD, Maryanti R. 2020. Understanding Archimedes' Law: What the Best Teaching Strategies for Vocational High School Students with Hearing Impairment. *Journal of Technical Education and Training*. 12(1): 299-237.

Kabanov A, Kramar V, Ermakov I. 2021. Design and Modeling of an Experimental ROV with Six Degrees of Freedom. *Drones*. 5(13): 1-19. DOI: https://doi.org/10.3390/drones5040113.

Konoplin A, Konoplin N, Yurmanov A. 2022. Development and Field Testing of a Smart Support System for ROV Operators. *Journal of Marine Science and Engineering*. 10(10): 1-14.

Kumar PA, Vasantha S, Hemaprabha G, Alarmelu S, Mohanraj K, Sreenivasa V, Gomathi R, Palaniswami C, Krishnapriya V, Anusha S, Alagupalamuthirsolai M, Vinayaka. 2023. Comparison of Stalk Volume by Water Displacement Method and Calculation Method for Stalk Weight Determination and Its Relevance to Single Cane Weight in Sugarcane Clones. *International Journal of Environment and Climate Change*. 13(8): 2282-2291. DOI: https://doi.org/10.9734/ijecc/2023/v13i82209.

Manullang S, Pusaka A, Setiawan A. 2020. The Preliminary of Design and Movement of Remotely Operated Vehicle (ROV). *2nd Maritime Safety International Conference (MASTIC), 18 Juli 2020, Surabaya*. IOP Conference Series: Earth and Environmental Science.

Payung M, Zain A. 2021. Rancang Bangun *Remotely Operated Vehicle* (ROV) untuk *Monitoring* Kondisi Terumbu Karang di Perairan Bontang. *Jurnal Nasional Komputasi dan Teknologi Informasi*. 4(2): 149-157. DOI: https://doi.org/10.32672/jnkti.v4i2.2838.

Prabowo Y, Broto S, Wisnuadji TW, Siswanto. 2022. Analisa Power Mode ESP32 untuk Catu Daya pada Sistem Berbasis IoT. *Prosiding Sistem Informasi dan Teknologi (SISFOTEK)*. 6(1): 150-154.

Rivalji JM. 2013. Design and Model Preparation of ROV to Define The Principle of Stability of A Submerged Body. *Proceedings of the 1st International Conference on Emerging Trends in Mechanical Engineering, January 4th-5th, 2013, Gujarat, India*. 383-388.

Ray S, Bhowal R, Patel P, Panaiyappan KA. 2020. A Close Look at Software Design Aspects of Remotely Operated Vehicles — A Survey. *2020 IEEE 4th Conference on Information & Communication Technology (CICT), 3-5 Desember 2020, Chennai, India*. 1-6.

Septian RA, Rahmania A, Nugraha MI, Yudhi. 2019. *Remotely Operated Vehicle* (ROV) untuk Eksplorasi Bawah Air di Lingkungan Industri Perkapalan. *Manutech: Jurnal Teknologi Manufaktur*. 9(2): 15-22. DOI: https://doi.org/10.33504/manutech.v9i02.41.

Xia P, McSweeney K, Wen F, Song Z, Krieg M, Li S, Yu X, Crippen K, Adams J, Du EJ. 2022. Virtual Telepresence for The Future of ROV Teleoperations: Opportunities and Challenges. *Proceedings of the 27th Offshore Symposium (SNAME), 22 Februari 2022, Houston*. 1-12.